Thermohydraulic Design Analysis Modeling for
Korea Advanced NUclear Thermal Engine Rocket for Space Application

Seung Hyun Nam[a*], Jae Young Choi[a], Paolo F. Venneri[a], Yong Hoon Jeong[a], Soon Heung Chang[a,b]

[a]Department of Nuclear and Quantum Engineering, Korea Advanced Institute of Science & Technology,
291 Daehak-ro, Yuseong-gu, Daejeon, Korea
[b]Handong Global University, Pohang-si, Gyeongbuk, Korea
[*]Corresponding author: rashkid@kaist.ac.kr

1. Introduction

Space exploration is a realistic and profitable goal for long-term humanity survival, although the harsh space environment imposes lots of severe challenges to space pioneers. To date, almost all space programs have relied upon Chemical Rockets (CRs) rating superior thrust level to transit from the Earth's surface to its orbit. However, CRs inherently have insurmountable barrier to carry out deep space missions beyond Earth's orbit due to its low propellant efficiency, and ensuing enormous propellant requirement and launch costs. Meanwhile, nuclear rockets typically offer at least two times the propellant efficiency of a CR and thus notably reduce the propellant demand. Particularly, a Nuclear Thermal Rocket (NTR) is a leading candidate for near-term manned missions to Mars and beyond because it satisfies a relatively high thrust as well as a high efficiency. The superior efficiency of NTRs is due to both high energy density of nuclear fuel and the low molecular weight propellant of Hydrogen (H_2) over the chemical reaction by-products. A NTR uses thermal energy released from a nuclear fission reactor to heat the H_2 propellant and then exhausted the highly heated propellant through a propelling nozzle to produce thrust. A propellant efficiency parameter of rocket engines is specific impulse (I_{sp}) which represents the ratio of the thrust over the propellant consumption rate. If the average exhaust H_2 temperature of a NTR is around 3,000 K, the I_{sp} can be achieved as high as 1,000 s as compared with only 450 ~ 500 s of the best CRs. For this reason, NTRs are favored for various space applications such as orbital tugs, lunar transports, and manned missions to Mars and beyond [1,2].

The best known NTR development effort was conducted from 1955 to1974 under the ROVER and NERVA programs in the USA. These programs had successfully designed and tested many different reactors and engines [3]. After these projects, the researches on NERVA derived NTR engines have continued as a main stream based on the mature technology. The typical core design of the NERVA derived engines uses hexagonal shaped fuel elements with circular cooling channels and structural tie-tube elements for supporting the fuel elements, housing moderator and regeneratively cooling the moderator. The state-of-the-art NTR designs mostly use a fast or epithermal neutron spectrum core utilizing a HEU fuel to make a high power reactor with small and simple core geometry. Meanwhile, innovative and futuristic NTR engine concepts of Korea Advanced NUclear Thermal Engine Rocket (KANUTER) were recently proposed to reduce the reactor size and mass or to implement a LEU fuel in the reactor by using thermal neutron spectrum. There are two versions of the KANUTER according to the fuel types with different Uranium enrichment as shown in Fig. 1. The HEU version is small and highly efficient engine [4,5], and the LEU version is non-proliferative and comparably efficient engine [6]. The KANUTERs have some features in the reactor design such as the integrated fuel element eliminating the typical tie-tube and the regeneratively cooling channels to enhance heat transfer in the core and ensuing rocket performance.

To study feasible design points in terms of thermo-hydraulics and to estimate rocket performance of the KANUTERs with the distinct reactor design, a new numerical NTR engine model, Nuclear Square-channel-core in Expander-cycle Simulation (NSES), is under development. This paper describes details of the NSES and also includes results of a preliminary thermo-hydraulic design analysis by using the model.
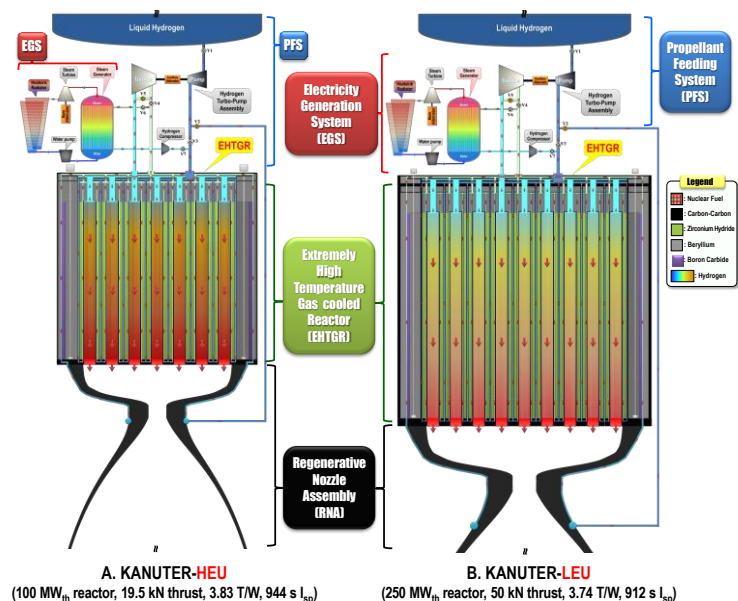

A. KANUTER-HEU
(100 MW_th reactor, 19.5 kN thrust, 3.83 T/W, 944 s I_sp)

B. KANUTER-LEU
(250 MW_th reactor, 50 kN thrust, 3.74 T/W, 912 s I_sp)

Fig. 1. Schematic view of the KANUTERs.

2. Description of KANUTER System

Overall, the KANUTERs consist of an Extremely High Temperature Gas cooled Reactor (EHTGR) utilizing H_2 propellant, a propulsion system, and an optional electricity generation system as depicted in Fig 1. The focal point of the KANUTER designs is the compact EHTGR with thermal neutron spectrum for the small and lightweight system or the LEU fuel utilization.

2.1 Moderated EHTGR

The cores of the EHTGRs mostly consist of the dozens of integrated fuel elements. The integrated fuel element uniquely houses the fuel assembly, moderator block, regeneratively cooling channel and structural components such as fuel support shroud and individual pressure tube as an all-in-one package as observed in Fig 2. The fuel assembly has the peculiar design of the square lattice geometry, which is first proposed by the Innovative Nuclear Space Power & Propulsion Institute (INSPI), to primary reduce the fabrication difficulties for creating micro cooling channels and to enhance the heat transfer in fuel [7]. As shown in Fig. 2, the grooved fuel wafers manufactured in thicknesses from 0.50 mm to 1.50 mm are interlocked with each other to form the square lattice geometry. The square lattice geometry creates numerous Square Flow Channels (SFC), which are Fuel Cooling Channels (FCC) maintaining 30% cross-sectional void fraction of the fuel assembly to ensure sufficient coolant passages and a critical fuel mass. This square lattice design is simple and cost-effective rather than the hexagonal fuel design having circular channels. In addition, the convective heat transfer capability of the SFC is higher than that of the circular channel with the same hydraulic diameter and heating because the heat transfer surface area of the SFC is as much as 27% larger, even though the averaged heat transfer coefficient of the SFC is about 10% lower [8]. As the fuel candidates of the EHTGRs, both (U, Zr, Nb)C solid solution with 93 w/o [235]U enrichment for the HEU version and [184]W-UO_2 CERMET with 19.5 w/o [235]U enrichment for the LEU version are considered. The ternary carbide fuel has higher operational temperature (around 3,000 K) and good neutronic characteristics, whereas the CERMET fuel has higher U density and improved creep strength despite its lower operational temperature (around 2,800 K). The moderator is absolutely crucial to reduce the heavy fuel demand and ensuing reactor mass, and to resultantly enable the LEU fuel use in the EHTGRs because it is able to strongly thermalize neutron spectrum. The suitable moderator candidates are the metal hydrides such as [7]Lithium Hydride ([7]LiH) or Zirconium hydride ($ZrH_{1.8}$) [9,10]. A serious challenge to use these hydride moderators in the high temperature core is to sufficiently cool them for prevention of melting and large H_2 dissociation. So, the fuel element contains the annular Moderator Cooling Channel (MCC) between the first fuel support shroud and the second moderator layers to protect the moderator from the thermal attacks in the core. The integrated design is also able to efficiently increase room for moderator in the core and to mitigate stress load to the pressure vessel (PV) by the individual pressure tube. The relative amounts of fuel and moderator are regulated by Pitch to Diameter ratio (P/D) of the fuel element.
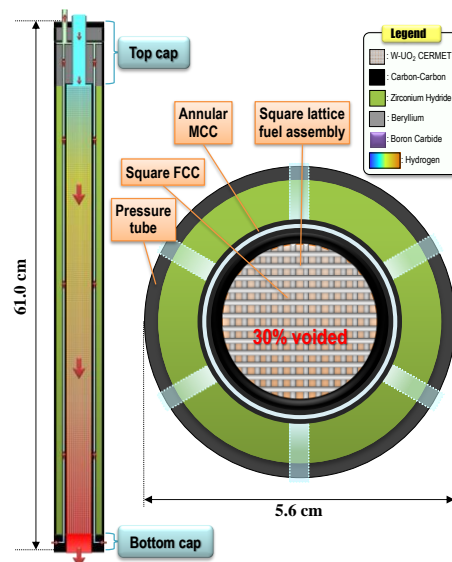

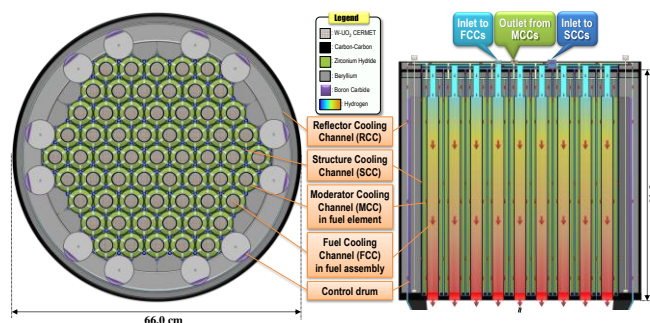Fig. 2. Configuration of the integrated fuel element.

Fig. 3. Configuration of the EHTGR-LEU.

The dozens of the integrated fuel elements arranged in the hexagonal prism pattern mainly compose the compact cores with the Beryllium (Be) spacers among the fuel elements as shown in Fig 3. The EHTGR-HEU has the 37 fuel elements in its small-size core and the EHTGR-LEU has the 61 fuel elements in the larger core. The Be spacers also have the Structure Cooling Channels (SCC) to cool the structural components and moderator at the outside of the fuel elements. The main structural materials are Carbon fiber-reinforced Carbon composite (C/C) and Be to reduce non-fission parasitic neutron absorption. The compact cores are surrounded by the reflector composed of the Be – Be – C/C layers to reduce neutron leakage. The last Be – C/C layers also serves as the reactor's PV [11]. The reflector has the annular Reflector Cooling Channel (RCC) as well. To control the reactor's reactivity, the cylindrical control drums are symmetrically placed in the reflector and comprise partially of Boron Carbide (B_4C) neutron absorber.

TABLE 1. Reference Design Parameters of the KANUTERs.

Category	KANUTER-HEU	KANUTER-LEU
EHTGR Parameters		
Power (electric power mode)	100 MW$_{th}$ (100 kW$_{th}$)	250 MW$_{th}$ (350 kW$_{th}$)
Number of fuel elements & P/D	37 & 2.00	61 & 1.62
Average fuel power density	14.7 MW$_{th}$/L	9.1 MW$_{th}$/L
Fuel type (^{235}U enrichment)	(U, Zr, Nb)C (93.0 wt%)	^{184}W-UO$_2$ CERMET (19.5 wt%)
Fuel & ^{235}U mass	48.6 & 9.1 kg	296.2 & 19.6 kg
Moderator type & mass	ZrH$_{1.8}$ & 92.7 kg	ZrH$_{1.8}$ & 124.3 kg
Structural material type	C/C and Be	
Reflector (PV) & control type	Be − Be − C/C & Control drums partially containing B$_4$C absorber	
Reactor diameter and height (core)	50.0 & 46.0 cm (32.9 & 32.9 cm)	66.0 & 51.0 cm (50.4 & 50.4 cm)
Rocket Performance		
Engine mass (excluding EGS)	516 kg	1,364 kg
- EHTGR	268 kg	727 kg
- Shadow shield & auxiliaries[*]	134 kg	363 kg
- Propulsion system[**]	114 kg	274 kg
Avg. chamber T and P	around 2,990 K & 6.895 MPa	around 2,826 K & 6.895 MPa
Thrust[***] and T/W$_{eng}$	19.5 kN & 3.86	50.0 kN & 3.74
Specific impulse	944 s	912 s
EGS Performance		
Power cycle option	Rankine (or Brayton)	
Thermal efficiency & power output	18.7 % & 15 kW$_e$	18.7 % & 55 kW$_e$
Radiator size	3.2 m^2/kW$_e$	

[*]Roughly predicted by 50 % of the reactor mass. [**]Predicted by rough scaling from the SNTP according to the powers and thrusts.
[***]Estimated at a nozzle expansion ratio of 200 and considering 5.5 % losses from ideal values.

The EHTGRs evenly distribute the protective and regenerative coolant channels in the cores such as the FCCs for fuel, MCCs and SCCs for moderator and structures, and RCC for reflector. The various cooling channels mitigate severe heating of the reactor components, whereas increase the coolant temperature to regeneratively transfer the heat to the power conversion systems for both propulsion and electricity generation. The EHTGRs could be operated in two modes of propulsion and electricity generation for the bimodal capability. In the propulsion mode, the reactors operate at full powers of a few hundred MW$_{th}$. In case of the electric power mode, the reactors operate at idle powers of several hundred kW$_{th}$. Table 1 includes the reference design parameters of the EHTGRs.

2.2 Bimodal Engine System

One of the NTR merits is that the system could be configured for the bimodal function of both propulsion and electricity generation. The bimodal NTR engines schematically shown in Fig 1 include the propulsion system and the optional Electricity Generation System (EGS) with the single heat source of the EHTGRs. Table 1 presents the reference design parameters and performance of the KANUTERs.

The propulsion system mainly comprises the Propellant Feeding System (PFS), the Regenerative Nozzle Assembly (RNA), etc. The key component of the PFS is the Turbo-Pump Assembly (TPA) to feed the propellant to the EHTGRs and in turn to the RNA. The TPA converts a small portion of thermal energy of the EHTGR into dynamic power to make the flow continue in the system.

Uniquely, the TPA is equipped with an auxiliary alternator to generate electricity in the propulsion mode or emergency. The RNA expands and accelerates the H$_2$ heated in the EHTGR to produce thrust. To protect the nozzle from the high temperature H$_2$, a small portion of the unheated propellant is passed through a regeneratively cooing jacket of the RNA. One of the RNA material options is a refractory carbide-coated C/C. The coated C/C nozzle is an innovative and feasible design because of its low weight and superior high-temperature strength largely reducing cooling requirement [12,13]. The expander cycle is selected for the propulsion system to convert the reactor heat to the powers for thrust, propellant feeding and electricity. In the expander cycle, the cold H$_2$ stream is pumped through the TPA and then splits up into both of the SCCs in the core, and the regeneratively cooling channel of the RNA and following the RCC. Most of the coolant flows into the core and the rest is used to cool the RNA and the reflector. The main stream after passing through the SCCs is connected with the annular MCCs at the bottoms of fuel elements, then flows into the reactor outlet head through the MCCs. Another core bypass stream also gathers into the reactor outlet head and is mixed with the main stream after cooling the RNA and the reflector. Then, the heated H$_2$ (around 300 K) flows out to the TPA for both propellant feeding and electricity generation. After the power conversion, the H$_2$ streams down into the FCCs in the core to be heated, and then expands out through the RNA to produce thrust.

The EGS converts the thermal energy of the EHTGR into the electric power in the electric power mode. In terms of high power and efficiency on the basis of

proven technology, both Brayton and Rankine cycles are the primary options for the EGS [14,15]. In a prospective study, the theoretical thermal efficiencies in a similar radiator size are respectively estimated at 6.4% at a pressure ratio of 1.50 and a turbine inlet temperature of 850 K for the Argon Brayton cycle, and 18.8% at a pressure ratio of 81 and a turbine inlet temperature of 670 K for the Toluene Rankine cycle. Then, the radiator sizes per electric power are 8.9 m^2/kW_e of the Brayton and 3.0 m^2/kW_e of the Rankine. The relatively low performance is mainly due to the systemic constraint that the maximum temperature at the turbine inlet is limited by the moderator's melting point. The result indicates that the thermal efficiency of the Brayton cycle is about 3 times lower than that of the Rankine cycle with the similar radiator area. However, the Rankine cycle must overcome the handling and separation issues of two-phase flow, which are problematic in zero-gravity.

3. Thermohydraulic Design Analysis Model

The model of the NSES currently focuses on thermo-hydraulic analysis of the complex EHTGR design during the propulsion mode in steady-state to estimate feasible design points and to study the effects of power and core geometry. The reactor design includes the peculiar square lattice fuel geometry and the various regeneratively cooling channels. The propulsion system is simply modeled as the expander cycle about the major components to obtain the input information for the reactor analysis and to estimate the theoretical engine performance including pump discharge pressure, pressure drop, chamber states, thrust, Thrust to Weight ratio (T/W$_{eng}$), I$_{sp}$, etc. The NSES includes 1-D thermodynamic model to estimate coolant states of the entire system and 2-D radial thermal conduction model to precisely predict temperature distribution in fuel. The NSES is written in MATLAB [16].

3.1 Major Engine Components and Heat Deposition

The engine system described in the NSES consists of both the propulsion system housing the liquid H$_2$ (LH$_2$) propellant tank, PFS, RNA, piping system and the EHTGR as a heat source as shown in Fig 4. The PFS mainly includes the TPA with a centrifugal pump, a turbine and an auxiliary alternator mounted on a same shaft for both propellant feeding and electric power generation. The RNA is a kind of converging-diverging nozzle with its regeneratively cooling jacket. The major components in the engine are connected with the piping system. The piping system includes various pipes, fittings, valves to control the bypass streams, distribution plenums and mixing junctions such as the reactor outlet head and the recombined points between the main and bypass streams. The components of the EHTGR are characterized with the equivalent coolant flow channels such as the FCC, MCC and SCC in the core, and the RCC in the reflector. The unit channels are respectively

represented by both the hot and averaged channels to consider the radial power distribution, and thus to estimate both the maximum pressure losses and the average enthalpy rises of coolant. To analyze temperature distribution of fuel, the hot-FCC includes the solid fuel domain which is used to describe the heat transfer by convection and conduction between the coolant and fuel.
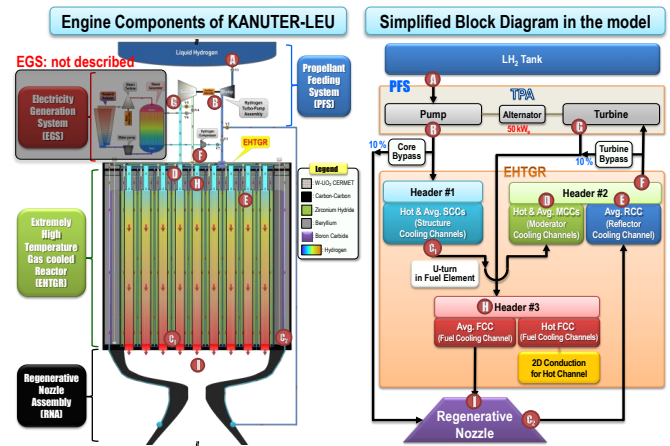

Fig. 4. The engine components described in the NSES and its simplified block diagram.

The locational variation in heat generation of each reactor component is described by the average heat deposition rate multiplied by the normalized power shape factors along the axial and radial location. The heat deposition data and the power profiles are determined by the preliminary neutronic analysis [6]. Then, it is assumed that the heat of each component is transferred to the corresponding cooling channel for simple analysis. For example, the heat of fuel is transferred to the FCCs except for the conducted heat to the fuel support shroud. The amount the conducted heat is estimated by the previous CFD analysis [17]. The heat transferred to the MCC is assumed to include both the heat depositions of the fuel support shroud, moderator, protective jacket of moderator and the conducted heat from fuel. The SCCs possesses the heat of the structural components such as the pressure tubes of fuel elements and the Be spacers in the core.

3.2 1-D Thermodynamic Model for Propellant Flow

The propellant flows through the components in order of (A) ~ (I) as described in Fig 4. To efficiently simulate the propellant flow in the entire system and ensuing power conversions for thrust, propellant feeding and electricity generation, the 1-D thermodynamic model is developed. Overall, the 1-D thermodynamic model consists of the conservation of continuity, momentum and energy, the pressure loss, the power conversion, and the ideal rocket equations as follows. The Equation Of State (EOS) is taken from the NIST REFPROP 9.0 at the temperature range down to 900 K [18] and the NASA Lewis chemical equilibrium based on the ideal gas assumption at the temperature range of over 900 K [19].

Conservations:

$$\rho_{in} A_{in} v_{in} = \rho_{out} A_{out} v_{out} = \dot{m}, \qquad (1)$$

$$P_{in} + \rho_{in} v_{in}^2 - \Delta P_f = P_{out} + \rho_{out} v_{out}^2, \qquad (2)$$

$$h_{in} + \frac{v_{in}^2}{2} + \frac{d\dot{Q}}{\dot{m}} = h_{out} + \frac{v_{out}^2}{2}. \qquad (3)$$

Major pressure loss: $\Delta P_f = f_D \frac{dL}{D_h} \frac{\bar{\rho}\bar{v}^2}{2}, \qquad (4)$

where $f_D \approx \frac{0.2479 - 0.0000947(7 - log_{10}\overline{Re})^4}{(log_{10}(\frac{\varepsilon}{3.615 D_h} + \frac{7.366}{\overline{Re}^{0.9142}}))^2}$ for turbulent flow.

Coil pressure loss: $\Delta P_f = f_C \frac{dL}{D_h} \frac{\bar{\rho}\bar{v}^2}{2}, \qquad (5)$

where $f_C = 0.336(\frac{D_h}{R})^{0.1} \overline{Re}^{-0.2}$ for turbulent flow.

Minor pressure loss: $\Delta P_f = K \cdot \frac{\rho_{in} v_{in}^2}{2}, \qquad (6)$

where K = geometric resistance coefficient.

Power conversion:

$$\dot{W}_{Pump} = \dot{m}(h_{out,a} - h_{in}), \qquad (7)$$

where $h_{out,a} = h_{in} + \frac{h_{out,s} - h_{in}}{\eta_{Pump}},$

$$\dot{W}_{Turb} = \dot{m}(h_{in} - h_{out,a}), \qquad (8)$$

where $h_{out,a} = h_{in} - \eta_{Turb}(h_{in} - h_{out,s}),$

$$PR_{Pump} = \frac{P_{out}}{P_{in}} \text{ and } PR_{Turb} = \frac{P_{in}}{P_{out}}, \qquad (9)$$

$$\dot{W}_{net} = \dot{W}_{Turb} - \dot{W}_{Pump}, \qquad (10)$$

$$\dot{W}_{elect} = \dot{W}_{net} * \eta_{Alt} = (\dot{W}_{Turb} - \dot{W}_{Pump})\eta_{Alt}. \qquad (11)$$

Ideal rocket:

$$\text{Area ratio} = \frac{A_{out}}{A_{thr}} = \frac{(\frac{2}{r+1})^{\frac{1}{r-1}}}{(\frac{P_{out}}{P_{cha}})^{\frac{1}{r}} \sqrt{\frac{r+1}{r-1}[1 - (\frac{P_{out}}{P_{cha}})^{\frac{r-1}{r}}]}}, \qquad (12)$$

$$v_{out} = \sqrt{\frac{2r}{r-1} R_{H_2} T_{cha} [1 - (\frac{P_{out}}{P_{cha}})^{\frac{r-1}{r}}] + v_{cha}^2}, \qquad (13)$$

$$F_{est} = \zeta_F F_{ide} = \zeta_F(\dot{m} v_{out} + P_{out} A_{out}), \qquad (14)$$

$$I_{sp} = \frac{F_{est}}{\dot{m} g_0}, \qquad (15)$$

$$T/W_{eng} = \frac{F_{est}}{m_{eng} g_0}. \qquad (16)$$

The propellant tank simply represents the thermo-dynamic state of the stored LH_2 which is also the inlet states of the pump in the analysis.

The TPA with the auxiliary alternator is simply modeled by Equations of (7) ~ (11) using the efficiencies of the subcomponents to only estimate the thermo-dynamic state, pressure ratios, shaft work and electric power generation. The efficiencies of the pump, turbine and alternator are assumed to be 0.65, 0.70 and 0.85, respectively. The Equations are iteratively solved with the EOS to first find the pressure ratio of the turbine.

The coolant flows in the complex piping system are modeled by Equations of (1) and (2) of conservations, and Equation (4) or (6) to estimate their pressure losses. In case of common pipes, the pressure losses are calculated by the Darcy–Weisbach (D-W) equation and the friction factors are predicted by the Colebrook approximation of

Equation (4) [20]. The minor pressure losses of the fittings, valves and distribution plenums are estimated by Equation (6) utilizing the geometric resistance coefficient (K). The values of the resistance coefficient are referenced from the CRANE engineering data [21]. Additionally, the mixing junctions, which are used two or more separate flows need to be combined into one, is modeled by both matching the outlet pressure to the lower of other inlet pressures and mass-averaging the inlet enthalpies to find the outlet temperature. The component models using the D-W equation are iteratively solved with the EOS to obtain average velocity and following pressure loss.

The EHTGR is described by the four equivalent cooling channels such as the FCC, MCC, SCC and RCC. The protective and regenerative coolant channels are also analyzed by the 1-D flow model in a constant area duct with heat addition and friction. The analysis of the cooling channels is performed by axially dividing them into many segments of constant wall temperature and numerically integrating the effects of heat addition and friction along the channel. Both the normalized power profile along the axial location and the power peaking factor at the radially central position are applied to describe the power distribution in the core. Additionally, non-uniform local mass flow rates in the core were employed according to the radial locations of the fuel elements to mitigate the non-optimized radial power peaking and ensuing local heat concentration [4]. The propellant flow of the cooling channels are iteratively solved by the conservations, Equations of (1) ~ (3), with the EOS to first estimate the outlet density. The pressure loss is also calculated by the D–W equation using the friction factor approximated by Equation (4). The geometry effects of the channels are reflected to the analysis by their hydraulic diameters. The values of surface roughness for the Colebrook approximation are conservatively assumed to be 1E-03 mm for the FCC and 3E-02 mm for the other cooling channels and the pipes.

The type of the RNA is assumed to be the heat-resistant C/C nozzle which could largely reduce the cooling requirement and thus have potential for even radiation cooling [13]. So, the amount of the core bypass flow to cool the RNA and the reflector could be assumed at to be 10 % of the system Mass Flow Rate (MFR) just for the regeneration. The channel-type of the regeneratively cooling jacket is assumed to be a kind of helical coil. The helical cooling channel is split into nine segments to consider variation in the radius of coil helix and the local heating for simple and subservient analysis. The amount of energy transferred from the nozzle wall to the unheated propellant for the regeneratively cooling is derived from the result of the previous CFD analysis [22]. The coolant flow in the helical cooling channel are also iteratively calculated by Equations of (1) ~ (3) and EOS, and its friction factor is predicted by Equation (5) [23] to just estimate thermodynamic state of the propellant. The converging-diverging nozzle is also simply modeled

by the ideal rocket Equations of (12) ~ (16) describing a quasi-1-D isentropic flow [24]. To conservatively approximate the nozzle performance, a thrust correction factor is applied to the thrust calculated for the ideal rocket. The thrust correction factor is assumed to be 0.945 (5.5 % losses to an ideal thrust).

3.3 2-D Radial Thermal Conduction Model for Fuel

To obtain the temperature distribution of the fuel with the complex square geometry, the 2-D radial thermal conduction model is developed. The model analyzes an axially discrete segment with constant heating of the FCC and numerically integrates the effects of the axial power distribution. The axial heat transfer between the segments is assumed to be negligible. The heat transfer model between the coolant and fuel comprises the convection equations including the empirical heat transfer correlation and the Finite-Difference Equations (FDEs) for 2-D radial thermal conduction as follows. The effective thermal conductivity of the W-UO$_2$ CERMET fuel is analytically predicted [25].

Convection: $d\dot{Q} = h_c A_w (\overline{T}_w - T_b),$ (17)

where $h_c = \frac{Nu k_{H_2}}{D_h}$, (18)

where $Nu = 0.021 Re^{0.8} Pr^{0.4} (\frac{\overline{T}_w}{T_b})^{-0.7} [1 + (\frac{d}{D_h})^{-0.7} (\frac{\overline{T}_w}{T_b})^{0.7}]$.

2-D conduction: $\dot{E}_{in} + \dot{E}_{gen} = 0,$ (19)

$\sum_{i=1}^{4} q_{(i) \to (m,n)} + \ddot{q}(\Delta x \cdot \Delta y \cdot 1) + q_{conv} = 0,$ (20)

General FDEs:

$T_{m,n-1} + T_{m,n+1} - 2T_{m,n} + \frac{\ddot{q}(\Delta x)^2}{2k_F} = 0,$ (21)

$2T_{m-1,n} + T_{m,n-1} + T_{m,n+1} - 4T_{m,n} + \frac{\ddot{q}(\Delta x)^2}{k_F} = 0,$ (22)

$T_{m-1,n} + T_{m,n-1} + T_{m,n+1} + T_{m+1,n} - 4T_{m,n} + \frac{\ddot{q}(\Delta x)^2}{k_F} = 0,$ (23)

$T_{m-1,n} + 2T_{m,n-1} + T_{m,n+1} + 2T_{m+1,n} - 6T_{m,n} + \frac{2h_c \Delta x}{k_F}(T_b - T_{m,n}) + \frac{3\ddot{q}(\Delta x)^2}{2k_F} = 0,$ (24)

$T_{m,n-1} + T_{m,n+1} + 2T_{m+1,n} - 4T_{m,n} + \frac{2h_c \Delta x}{k_F}(T_b - T_{m,n}) + \frac{\ddot{q}(\Delta x)^2}{k_F} = 0.$ (25)

The local heat transfer coefficient and ensuing average wall temperature of a discrete segment are calculated by Equations (17) and (18). The heat transfer correlation, which is specified for turbulent heat transfer in a square duct, could predict the coefficient of the square FCC more exactly and conservatively (about 10% below) than that of corresponding circular channel [8,26].

The 2-D radial thermal conduction model for the solid domain with heat generation uses the energy balance method to develop the FDEs in steady-state condition. In the energy balance method, the FDE for a node is obtained by applying conservation of energy to a control volume about the nodal region as shown in Equations (19) and (20). Consequentially, the general FDEs pertinent to the five common geometries are

Equations of (21) ~ (25) for the situations of internal heating and Δx=Δy as depicted in Fig. 5. Then, for the unit channel of one quarter the FCC, all 13 FDEs are developed to obtain the temperature distribution of the square channel with the 13 node types. The 13 FDEs are directly solved with average thermal conductivity of fuel by the matrix inversion method utilizing computational calculation.
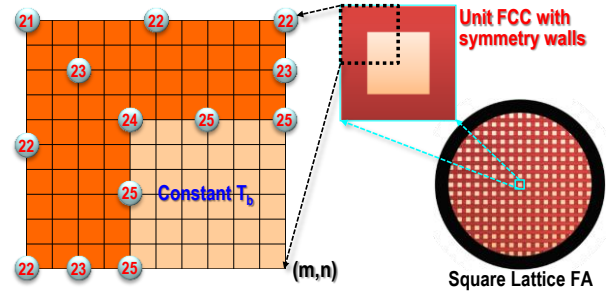

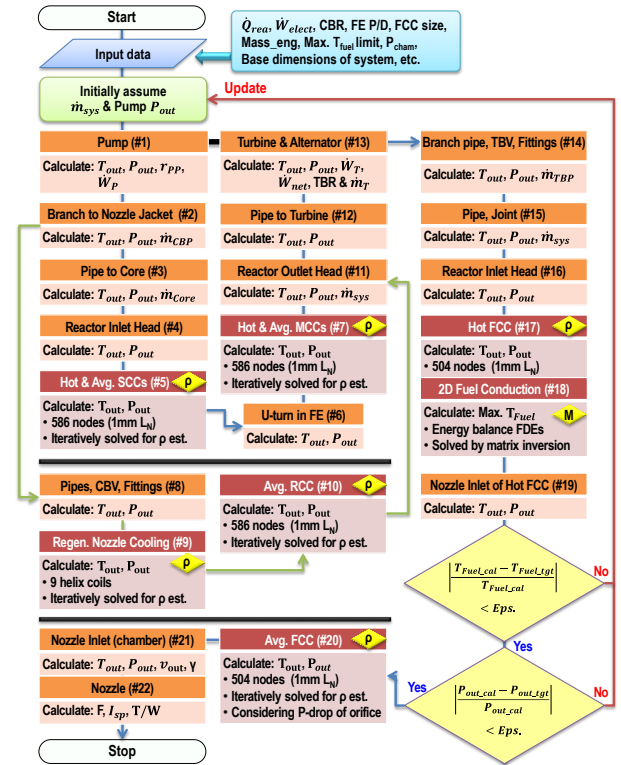Fig. 5. The unit channel for the fuel conduction model.

Fig. 6. Computational analysis process in the NSES.

3.4 Computational Analysis Process

Fig. 6 briefly presents the computational analysis process of the NSES. The code iteratively solves the component models (steady state) in order based on initial conditions. The input data includes reactor power, required electric power, both coolant bypass ratios before the inlets of the core and the turbine, P/D of the fuel element, size of the unit FCC, base dimensions of the system components, etc. For the fuel geometry effect analysis of the KANTER-LEU [6], the constant values in the input data are the reactor power of 250

MW_{th}, the corresponding P/D of 1.62, the required electric power of 50 kW_e, the same bypass ratios of 0.10, and the base dimensions of the system. Then, the variable is the FCC size of the square lattice fuel assembly: five FWTs of 0.50 ~ 1.50 mm. The iterative calculation ends when both peak temperature of the hot-FCC and average chamber pressure meet their target values of 2,990 K and 6.895 MPa, respectively. As the design criterion for the analysis, the peak temperature limit of fuel's centerline is set to ensure 150 K margin for the melting point of UO_2 (3,140 K). The maximum system pressure limit is set to be 16 MPa considering 80% margin for a high-level pump discharge pressure (20 MPa) at the constant chamber pressure (6.895 MPa) of typical expander engines [1]. Then, the final outputs are MFR, thermodynamic states of the components and resultant rocket performance such as thrust, T/W and I_{sp}.

4. Preliminary Thermohydraulic Design Analysis

The fuel geometry effect analysis was carried out on the KANUTER-LEU. The key variable is the size of the FCC with the FWTs from 0.50 mm to 1.50 mm to verify the cooling capability of the unique square lattice fuel design and thus to estimate the states of core and thrust chamber, and resultant rocket performance [6]. The reactor power is assumed to be the highest value of 250 MW_{th} to find the design points ensuring the maximum rocket performance. As the characteristic of the square lattice fuel design, the size of FCC determines the number of SFCs and the related heat transfer area per unit fuel volume. The thicker FWT of FCC decreases

the number of SFCs and the ensuing heat transfer area in the form of a negative exponential curve as shown in Fig. 7.

Both drop of the heat transfer area and corresponding growth of the distance between the fuel centerline and coolant by the thicker FWT strongly increase the peak temperature in the fuel centerline. When the peak temperature is over the temperature limit of fuel, the NSES automatically increases the coolant MFR to decrease the peak fuel temperature to the limit point through the iterative solving process. Accordingly, the MFR of system and the average temperature of chamber are changed depending on the FWTs in the limited peak fuel temperature as depicted in Fig. 8. The maximum temperature difference between the fuel and the chamber also exponentially increases with the FWT thickening. The highest temperature of the chamber (2826.6 K) is rated at the thinnest FWT of 0.50 mm and the lowest MFR of 5.587 kg/s. On the contrary, the lowest chamber temperature falls to 2,331.5 K at the thickest FWT of 1.50 mm and the largest MFR of 7.018 kg/s. Fig. 9 compares the temperature distributions along the axial location in the hot-FCCs with the FWTs of 0.50 mm, 1.00 mm and 1.50 mm, respectively. In case of the thinnest FWT of 0.50 mm, the temperature differences among the fuel centerline, the fuel surface and the bulk coolant along the axial locations are relatively small. However, the thicker FWT drastically expands the temperature differences and resultantly causes the peaking shapes of the fuel temperatures similarly following the axial power distribution.
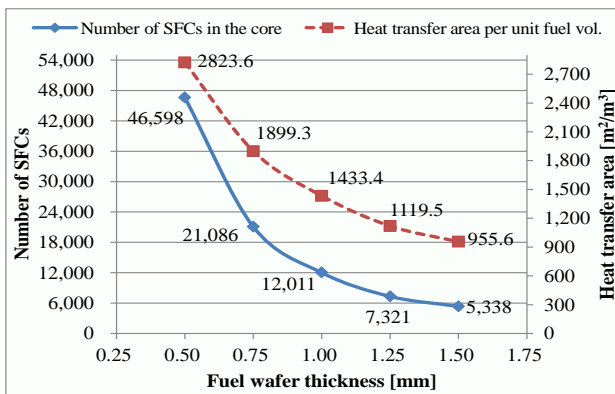

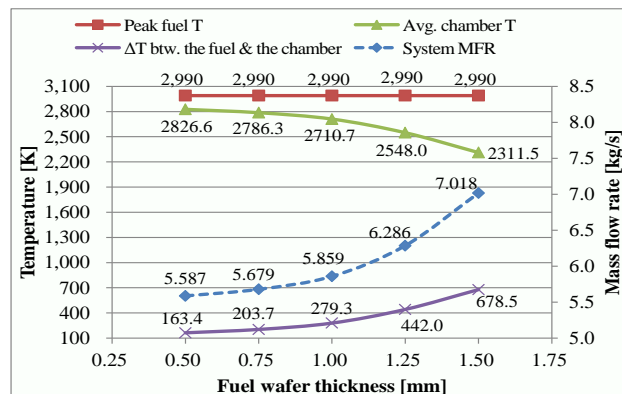Fig. 7. Number of SFCs and heat transfer area as a function of the FWT.

Fig. 8. Temperatures versus MFR as a function of the FWT.

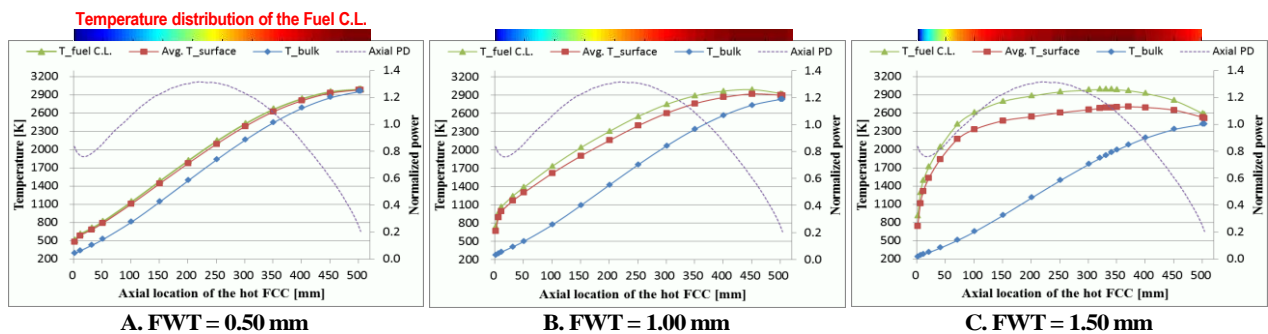**A. FWT = 0.50 mm**　　　　**B. FWT = 1.00 mm**　　　　**C. FWT = 1.50 mm**

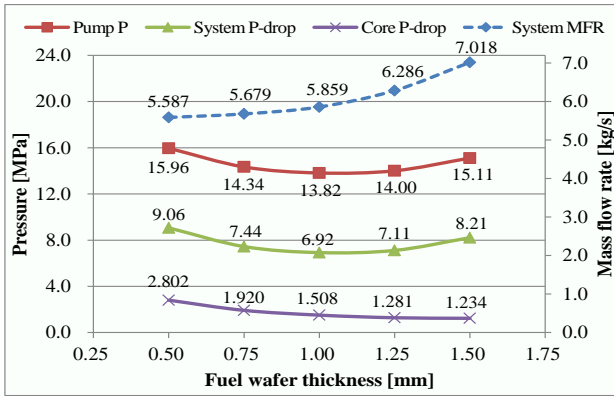Fig.9. Temperature distributions along the hot-FCC as a function of the FWT.

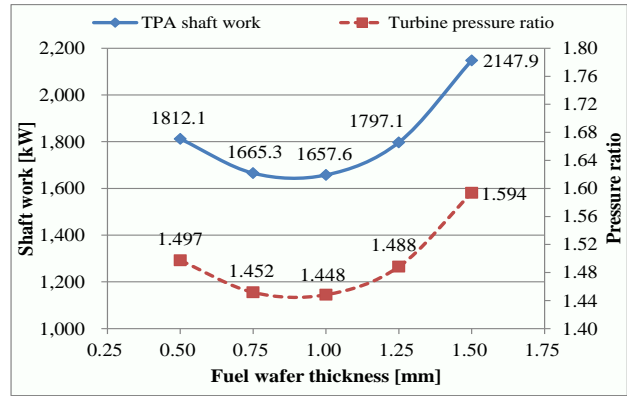Fig. 10. Pressures versus MFR as a function of the FWT.

Fig. 11. Shaft work and turbine pressure ratio of the TPA as a function of the FWT.
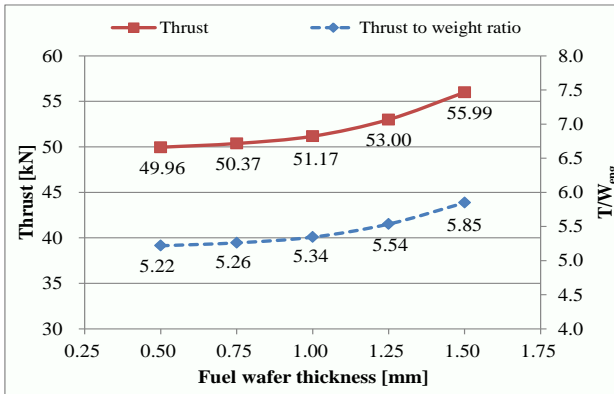

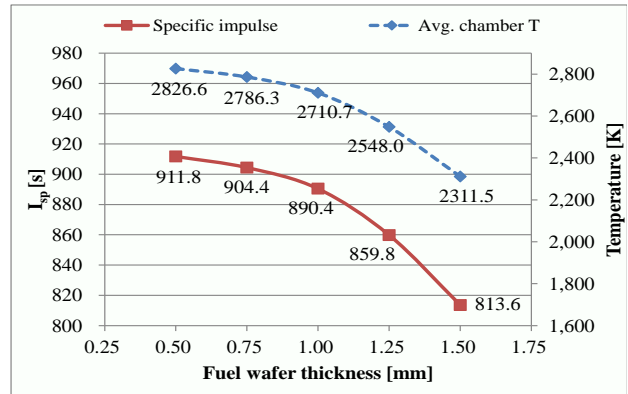Fig. 12. Thrust and T/W$_{eng}$ as a function of the FWT.

Fig. 13. I$_{sp}$ versus T$_{chamber}$ as a function of the FWT.

The pressure changes of the system are also unique, which shows the positive quadratic behavior according to the FWT thickening as presented in Fig. 10. The pressure drop of the core slightly decreases with the FWT increasing because the frictional surface area of the FCC exponentially drops, even though the MFR is augmented. This result shows the effect of the fuel surface area on the core pressure drop is slightly larger than that of the amount of the MFR increasing. However, the pump discharge pressure and the system pressure drop decrease to the lowest points at the FWT of 1.00 mm, and make an upward reverse with the further FWT increasing. Additionally, the shaft work of the TPA and corresponding pressure ratio of the turbine also plot the similar positive quadratic curves according to the FWT increasing as depicted in Fig. 11. These phenomena indicates that the decreasing effect of the core pressure drop is dominant on the system pressure up to the FWT of 1.00 mm, whereas the increasing effect of the pressure drop by the MFR rise in the other components overwhelms the decreasing effect of the core pressure drop at over the FWT of 1.00 mm. The maximum system pressure and core pressure drop are 15.96 MPa and 2.80 MPa at the thinnest FWT of 0.50 mm, while their minimum values respectively drop to 13.82 MPa and 1.51 MPa at the FWT of 1.00 mm.

In case of the rocket performance, according to the growth of the FWT, the thrust and T/W shown in Fig. 12 slightly increase mainly due to the MFR rise,

whereas the I$_{sp}$ observed in Fig. 13 rapidly decreases primarily due to the temperature drop of the chamber. Overall, the maximum chamber temperature and corresponding I$_{sp}$ are 2826.6 K and 911.8 s at the thinnest FWT of 0.50 mm, whereas the minimum system pressure and the relatively high thrust and T/W are 13.82 MPa, 51.2 kN and 5.34, respectively, at the FWT of 1.00 mm. Therefore, in the viewpoint of high propellant efficiency, the thinnest FWT of 0.50 mm is the best choice. On the other hand, in both viewpoints of lower system pressure and relatively high thrust, the FWTs of 0.50 ~ 1.00 mm are adequate. Fig. 14 presents the thermodynamic state of the components according to the FWTs of 0.50 ~ 1.00 mm.
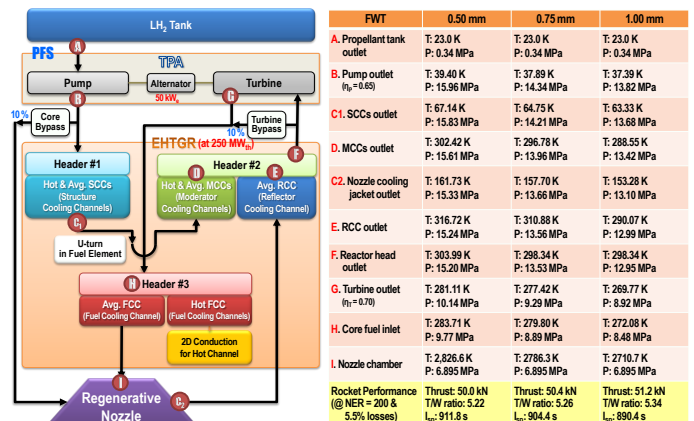

Fig. 14. Thermodynamic state of the components

5. Conclusions

Nuclear propulsion is the most promising and viable option to achieve challenging deep space missions. Particularly, the attractions of a NTR include excellent thrust and propellant efficiency, bimodal capability, proven technology, and safe and reliable performance. The KANUTER-HEU and -LEU are the innovative and futuristic NTR engines to reduce the reactor size and to implement a LEU fuel in the reactor by using thermal neutron spectrum. The KANUTERs have some features in the reactor design such as the integrated fuel element and the regeneratively cooling channels to increase room for moderator and heat transfer in the core, and ensuing rocket performance.

To study feasible design points in terms of thermo-hydraulics and to estimate rocket performance of the KANUTERs, the NSES is under development. The model of the NSES currently focuses on thermo-hydraulic analysis of the peculiar and complex EHTGR design during the propulsion mode in steady-state. The NSES written in MATLAB includes the 1-D thermo-dynamic model to estimate coolant states of the entire system and the 2-D radial thermal conduction model to precisely predict temperature distribution in fuel. The preliminary design analysis to study the fuel geometry effects on the KANUTER-LEU was carried out by using the NSES. The results indicate comparable performance for future applications, even though it uses the heavier LEU fuel.

In future, the NSES will be modified to obtain temperature distribution of the entire reactor components and then more extensive design analysis of neutronics, thermohydraulics and their coupling will be conducted to validate design feasibility and to optimize the reactor design enhancing the rocket performance.

REFERENCES

[1] E.S. Pedersen, Chapter 6. Nuclear Rocket Engine Design, in:, Nuclear Energy in Space, Prentice-Hall, Inc., Englewood Cliffs, NJ, USA, 1964: pp. 184–252.

[2] B.P. Bromley, Nuclear Propulsion: Getting More Miles Per Gallon, Astrodigital. (2000).

[3] S. Gunn, Nuclear propulsion - a historical perspective, Space Policy. 17 (2001) 291–298. doi:10.1016/S0265-9646(01)00044-3.

[4] S.H. Nam, J.I. Lee, S.H. Chang, Preliminary Thermo-hydraulic Core Design Analysis of Korea Advanced Nuclear Thermal Engine Rocket for Space Application, in: Transactions of the Korean Nuclear Society Spring Meeting, KNS, Korea, 2014.

[5] P. Venneri, S.H. Nam, Y. Kim, Neutronics Study of KANUTER Space Propulsion Reactor, in: Transactions of the Korean Nuclear Society Spring Meeting, KNS, Jeju, Korea, 2014.

[6] S.H. Nam, P.F. Venneri, J.Y. Choi, Y.H. Jeong, S.H. Chang, Preliminary Design Study of an Innovative High-Performance Nuclear Thermal Rocket Utilizing LEU Fuel, in: Proceedings of Nuclear and Emerging Technologies for Space 2015, ANS, Albuquerque, NM, USA, 2015.

[7] S. Anghaie, T.W. Knight, J. Plancher, R. Gouw, Development of a Robust Tri-Carbide Fueled Reactor for Multi-Megawatt Space Power and Propulsion Applications, INSPI, University of Florida, Gainesville, FL, USA, 2004.

[8] E. Battista, H. Perkins, Turbulent heat and momentum transfer in a square duct with moderate property variations, International Journal of Heat and Mass Transfer. 13 (1970) 1063–1065.

[9] R. E. Hyland, Reactor-Weight Study of Beryllium Oxide, Beryllium, Lithium-7 Hydride, and Water as Moderators with Tungsten184 Structural Material and Uranium Dioxide Fuel, NASA/TN D-1407, 1962.

[10] C.D. Montgomery, Fabrication and properties of lithium hydride, Nuclear Engineering and Design. 25 (1973) 309–314.

[11] J. Powell, J. Paniagua, G. Maise, H. Ludewig, M. Todosow, The Role of Compact Nuclear Rockets in Expanding the Capability for Solar System Science and Exploration, State University of New York at Stony Brook/TR-740, Stony Brook, NY, USA, 1997.

[12] S. Locke, R. Ahearn, Material Design Concepts for Uncooled Nuclear Rocket Nozzles, Materials Science Research. (1965) 287–310.

[13] R. Haslett, Space Nuclear Thermal Propulsion Program - Final Report, Bethpage, NY, USA, 1995.

[14] A.K. Hyder, R.L. Wiley, G. Halpert, D. f. Flood, S. Sabripour, Chapter 7. Dynamic Energy Conversion, in: Spacecraft Power Technologies, Imperial College Press, London, UK, 2000: pp. 323–351.

[15] G.L. Bennett, R.J. Hemler, A. Schock, Status report on the U.S. space nuclear program, Acta Astronautica. 38 (1996) 551–560.

[16] MathWorks, MATLAB, (2014).

[17] S.H. Nam, S.G. Kang, I.K. Jung, K.Y. Suh, Computational Thermohydrodynamic Analysis of Thermal Engine Rocket Adventurer for Space Nuclear Application, in: 2008.

[18] NIST, NIST Reference Fluid Thermodynamic and Transport Properties Database (REFPROP), (2010).

[19] S. Gordon, B.J. Mcbride, Computer Program for Calculation of Complex Chemical Equilibrium compositions and Applications, NASA/RP-1311, 1994.

[20] G. Papaevangelou, C. Evangelides, C. Tzaimopoulos, A New Explicit Relation for the Friction Coefficient in the Darcy-Weisbach Equation, in: Protection and Restoration of the Environment, Corfu, Italy, 2010.

[21] Crane Co., Flow of Fluids Through Valves, Fittings, and Pipe (TP-410), Crane, 2009.

[22] S.H. Nam, K.Y. Suh, Conceptual Design of Thermal Engine Rocket Adventurer for Space Nuclear Application., Seoul National University, 2009.

[23] Neutrium, Friction Factor for Flow in Coils and Curved Pipe, Neutrium. (2012).

[24] G. Sutton, O. Biblarz, Chapter 3. Nozzle Theory and Thermodynamic Relations, in: Rocket Propulsion Elements, Seventh Ed, JOHN WILEY & SONS, INC., NY, USA, 2011: pp. 45–101.

[25] J. a. Webb, I. Charit, Analytical determination of thermal conductivity of W–UO2 and W–UN CERMET nuclear fuels, Journal of Nuclear Materials. 427 (2012) 87–94.

[26] M.F. Taylor, Correlation of local heat transfer coefficients for single phase turbulent flow of hydrogen in tubes with temperature ratios to 23, NASA TN D-4332, 1968.